Supporting Information

Olson et al. 10.1073/pnas.0910283107

Importance of MMPs in Tumor Biology and Pathology

MMP-2 and -9 are proteases whose activity is intimately involved in the process of tumor invasion and metastasis in a wide range of tumor cell lines and clinical examples, a few of which are cited below (1–5). The role of MMPs in neovascularization and angiogenesis has been nicely reviewed (6). MMPs have been closely linked to epithelial-mesenchymal transitions (EMT) in both directions: MMPs can cause EMT (7, 8), and transcription factors known to drive EMT also stimulate MMP expression (9–13).

Synthesis of Peptide 1. Suc-e_8-(Aop)-PLGC(Me)AG-r_9-c-NH_2 was synthesized via standard Fmoc solid phase peptide synthesis. Suc represents succinyl, lowercase letters represent D-amino acids, (Aop) represents 5-amino-3-oxapentanoyl, C(Me) is S-methylcysteine, and the final NH_2 indicates C-terminal amide. The N-terminal succinyl group was added to the peptide by reaction with succinic anhydride while still on resin. The peptide was cleaved from the resin in a standard mixture (trifluoroacetic acid with 2% each of thioanisole, triisopropylsilane, and ethandithiol) overnight at room temperature. Most of the trifluoroacetic acid was removed by rotary evaporator, 50% hexanes in diethyl ether was added, and the peptide was collected by centrifugation. The collected solid was washed with 50% hexanes in ether three times and vacuum dried overnight. The peptide was purified on high performance liquid chromatography (HPLC) using 15–30% acetonitrile in water and 0.05% TFA, giving 30% yield from the crude peptide. The correct purified product was confirmed by electrospray mass spectroscopy: calculated 3271.5 Da, found 3271.8.

Synthesis of Peptide-Labeled Dendrimer 2. Twenty-five milligrams of peptide 1 was dissolved in 2 mL DMSO under N_2 was reacted with 2.3 mg 2-nitro-4-sulfophenyl 6-maleimidohexanoate sodium salt and 20 μl N-methylmorpholine. After stirring at room temperature for 3 h, liquid chromatography-mass spectroscopy (LC-MS) analysis of the reaction mixture indicated over 90% completion. The reaction mixture was cooled to 0 °C, 150 mg PAMAM dendrimer (Generation 5, with free amino groups, supplied by Dendritic Nanotechnologies as a 10% solution in methanol) and 2 mL 1 M HEPES buffer (pH 7.8) were added and stirred at 5 °C for 2 days. The reaction mixture was used directly in the next step.

Synthesis of Cy5- and Peptide-Labeled Dendrimer 3. Cy5 mono(N-hydroxysuccinimide) (1.2 mg) was added to the preceding reaction mixture and stirred at 5 °C overnight. The reaction mixture was used directly to make dendrimers 4 and 5.

Synthesis of Capped Cy5- and Peptide-Labeled Dendrimer 4. MeO$(CH_2CH_2O)_3CH_2CH_2CO$-(N-hydroxysuccinimide)ester (mPEG4 NHS ester, 166 mg, Quanta Biodesign) was added to reaction mixture 3 at 5 °C and stirred at that temperature for 3 days. The crude product was diluted with 10 mL water, and low molecular weight contaminants removed by filtration eight times through a membrane with 10 kDa cutoff. HPLC using a size-exclusion column (BioSep-SEC-S 3000 from Phenomenex, 300 × 7.5 mm, 1 mL/ min flow rate, water with 0.5% TFA as solvent, detection at 650 nm) indicated 99% purity, 72% yield. An average of three fluorophores per dendrimer was determined by dissolving a known weight of purified final product in water and measuring the Cy5 absorbance at 650 nm, assuming an extinction coefficient of 250,000 $M^{-1}cm^{-1}$. Static multiangle light scattering at 785 nm (Dawn-8, Wyatt Technology) indicated an apparent molecular weight of 72.9 kDa. Dynamic light scattering (Wyatt QELS) at 785 nm indicated a hydrodynamic radius of 4.6 nm.

Scheme 1

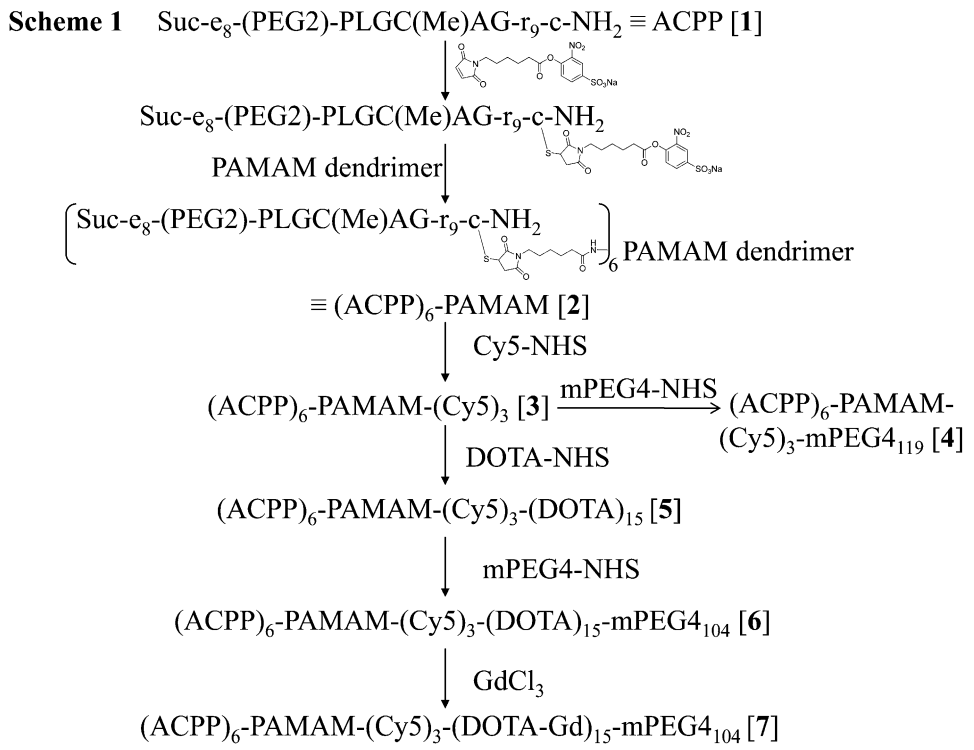

Synthesis of DOTA-, Cy5-, and Peptide-Labeled Dendrimer 5. Thirty equivalents of DOTA mono-N-hydroxysuccinimide ester (Macrocyclics Inc.) in HEPES buffer were reacted with reaction mixture 3 overnight at 5 °C. The reaction mix was used directly for the next step.

Synthesis of Capped DOTA-, Cy5-, and Peptide-Labeled Dendrimer 6. Reaction mixture 5 was reacted with 950 equivalents mPEG4 NHS ester and stirred at 5 °C for 3 days. The crude product was purified as described for 4, then lyophilized. 78% yield.

Gd Loading of 6. Twenty-five milligrams 6 dissolved in 1 mL 0.5 M ammonium acetate and 1 mL water was mixed with 100 μL 0.5 M $GdCl_3$ and stirred at room temperature for 3 days shielded from light. Small molecules were eliminated by five aqueous washes, removing excess water by centrifugation through a membrane filter with 10-kDa cutoff. Finally the Gd-loaded product 7 was lyophilized overnight to give a blue fluffy solid. The pure product was weighed and redissolved in water to give a 200 μM solution. A measured small aliquot was mixed with 0.5 mL concentrated nitric acid for 2 h, and then sent to Bodycote Analytical Services for Gd quantitation by ICP-MS, which indicated an average of 15 Gd per dendrimer. The number of Cy5 labels per dendrimer was confirmed to be three, based on 65-nm absorbance.

D-Amino acid controls were made by the same procedure but with D-amino acids in the hexapeptide linker. Because Fmoc-D-(S-methyl)cysteine was not commercially available, it was synthesized by methylation of Fmoc-D-cysteine.

1. Egeblad M, Werb Z (2002) New functions for the matrix metalloproteinases in cancer progression. *Nat Rev Cancer* 2:161–174.
2. Määttä M, Soini Y, Liakka A, Autio-Harmainen H (2000) Differential expression of matrix metalloproteinase (MMP)-2, MMP-9, and membrane type 1-MMP in hepatocellular and pancreatic adenocarcinoma: Implications for tumor progression and clinical prognosis. *Clin Cancer Res* 6:2726–2734.
3. Chen X, et al. (2005) Increased plasma MMP9 in integrin alpha1-null mice enhances lung metastasis of colon carcinoma cells. *Int J Cancer* 116:52–61.
4. Jinga DC, et al. (2006) MMP-9 and MMP-2 gelatinases and TIMP-1 and TIMP-2 inhibitors in breast cancer: Correlations with prognostic factors. *J Cell Mol Med* 10:499–510.
5. Gorden DL, et al. (2007) Resident stromal cell-derived MMP-9 promotes the growth of colorectal metastases in the liver microenvironment. *Int J Cancer* 121:495–500.
6. Berndt S, Bruyère F, Jost M, Noël A (2008) Chapter 16: In vitro and in vivo models of angiogenesis to dissect MMP functions. In *The Cancer Degradome*, eds Edwards D, Høyer-Hansen G, Blasi F, Sloane BF (Springer, New York), pp 305–325.
7. Orlichenko LS, Radisky DC (2008) Matrix metalloproteinases stimulate epithelial-mesenchymal transition during tumor development. *Clin Exp Metastasis* 25:593–600.
8. Radisky DC, et al. (2005) Rac1b and reactive oxygen species mediate MMP-3-induced EMT and genomic instability. *Nature* 436:123–127.
9. Tester AM, Ruangpanit N, Anderson RL, Thompson EW (2000) MMP-9 secretion and MMP-2 activation distinguish invasive and metastatic sublines of a mouse mammary carcinoma system showing epithelial-mesenchymal transition traits. *Clin Exp Metastasis* 18:553–560.
10. Rowe RG, et al. (2009) Mesenchymal cells reactivate Snail1 expression to drive three-dimensional invasion programs. *J Cell Biol* 184:399–408.
11. Joseph MJ, et al. (2009) Slug is a downstream mediator of transforming growth factor-beta1-induced matrix metalloproteinase-9 expression and invasion of oral cancer cells. *J Cell Biochem* 108:726–736.
12. Jin H, et al. (2009) Snail is critical for tumor growth and metastasis of ovarian carcinoma. *Int J Cancer*, 10.1002/ijc.24901.
13. Ota I, Li XY, Hu Y, Weiss SJ (2009) Induction of a MT1-MMP and MT2-MMP-dependent basement membrane transmigration program in cancer cells by Snail1. *Proc Natl Acad Sci USA* 106:20318–20323.

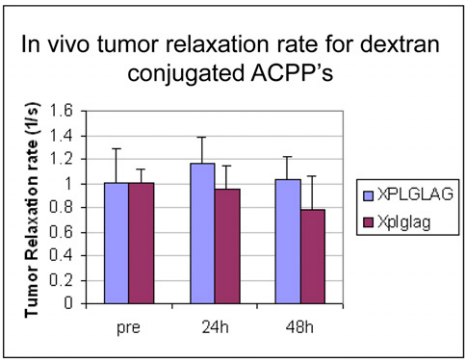

Fig. S1. Magnetic resonance imaging results with 70 kDa aminodextrans carrying single ACPP-DOTA(Gd) conjugates. Blue bars indicate proton relaxation rates $R_1 = 1/T_1$ in HT1080 tumor xenografts, before and 24 or 48 h after injection of 250 nmol of the aminodextran conjugate shown below. Red bars indicate analogous measurements from a MMP-resistant control, in which the cleavage sequence PLGLAG was replaced by the D-amino version plglag. T_1 values were obtained by varying T_r, taking five data points and fitting the resultant curve to Intensity = $A(1-\exp(1-T_r/T_1))$. The lack of significant differences between post- and preinjection R_1 values or between cleavable and uncleavable sequences argued that attachment of the macromolecule (e.g., 70 kDa dextran) and a single Gd complex, respectively to the polyglutamate and polyarginine ends of the ACPP failed to deliver enough Gd reliably into the tumor.

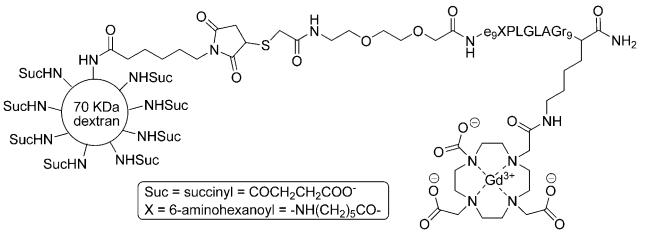

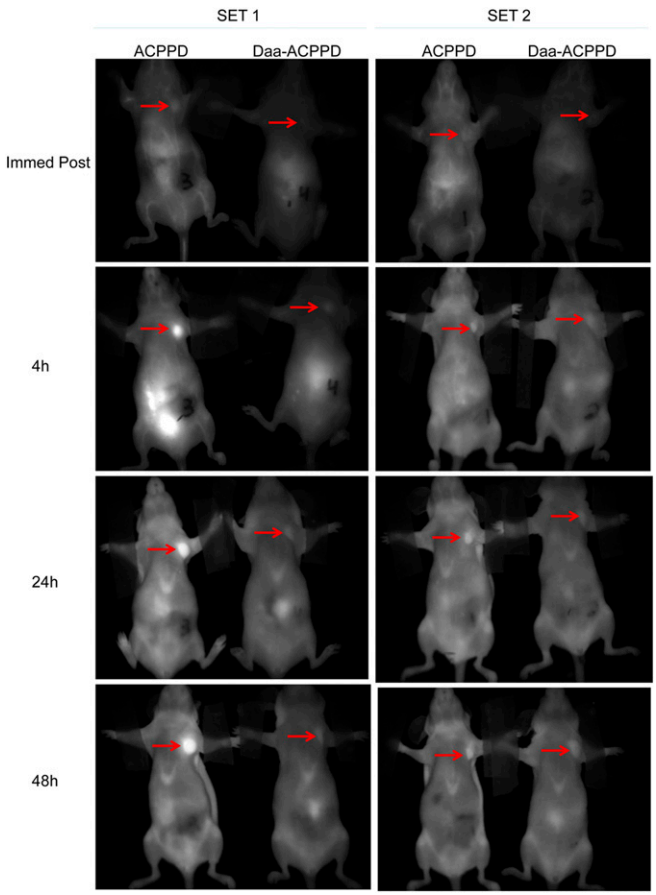

Fig. S2. Mice bearing HT-1080 xenografts imaged through intact skin a few minutes, 4, 24, and 48 h after injection with cleavable or D-amino acid control ACPPD-Cy5 as indicated. Two sets of animals are shown, one set with relatively large tumors and one set with much smaller tumors. All images are shown with the same intensity scaling. In in vivo images, tumor fluorescence intensity varies with tumor size and geometry as well as with MMP activity.

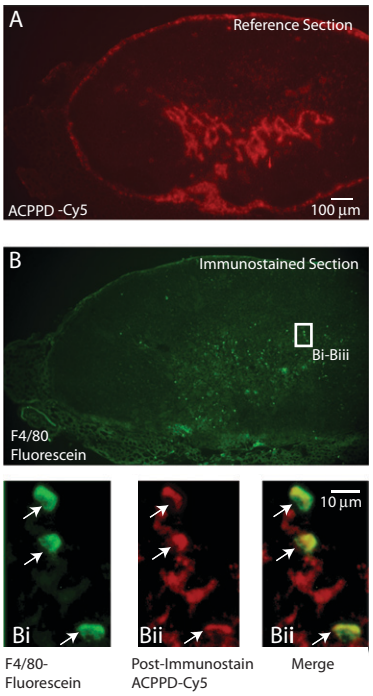

Fig. S3. ACPPD's are taken up by sinusoidal macrophages in reactive lymph nodes draining tumor beds from a mouse bearing an HT-1080 tumor. (*A*) Dual ACPPD uptake of a lymph node under Cy5 fluorescence. Most of the uptake is confined to sinusoids in the interior of the lymph node. (*B*) A separate section from the same lymph node after immunostaining for F4/80, a standard molecular marker for mature macrophages. (*Inset*) white box is shown at higher magnification in panels *Bi–Biii*. *Bi* shows three separate cells with dense F4/80 immunoreactivity. *Bii* shows the residual ACPPD- Cy5 signal from the same section after immunostaining. *Biii* is an overlay of *Bi* and *Bii*, showing that many but not all of the cells that accumulate ACPPD-Cy5 fluorescence are mature macrophages (F4/80 positive cells).

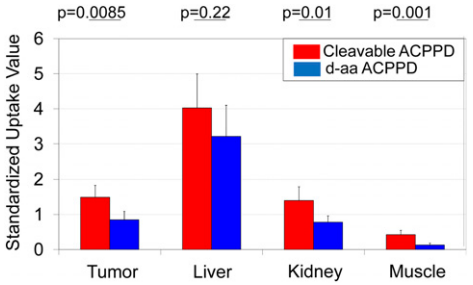

Fig. S4. Standardized uptake values for MMTV-PyMT mice 48 h after injection with cleavable ($n = 6$) and D-amino acid control ($n = 4$) ACPPD-Cy5's. P-values from pairwise t-tests are shown for each individual organ.

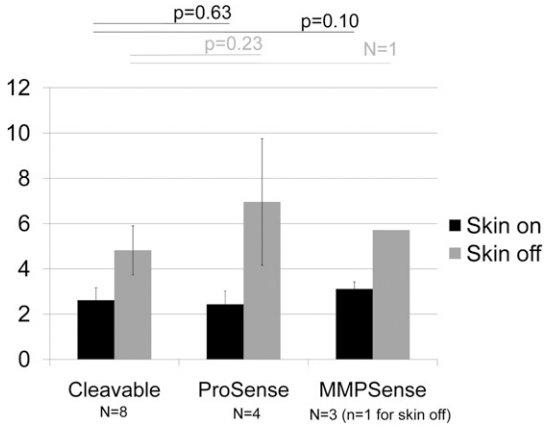

Fig. S5. Tumor to "background" ratios comparing cleavable ACPPD-Cy5's to ProSense and MMPSense in an HT-1080 xenograft model. For animals with intact skin, background represents skin on the contralateral side of the thorax. For animals with skin removed, background represents thoracic muscle on the contralateral side of the animal. Variation is largely due to tumor size, position and shape as shown in Fig. S2. SUVs cannot be assessed for ProSense and MMPSense because protease activity increases the fluorescence quantum efficiency of the dyes rather than tissue uptake and because the dye concentration cannot be deduced from the final fluorescence of a tissue homogenate.

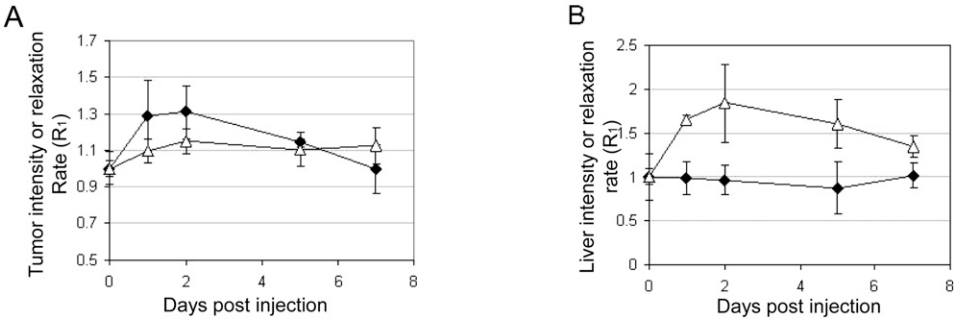

Fig. S6. Uptake of an ACPPD-Gd in PyMT mice normalizes over 7 days. (*A*) Tumor intensities (open triangles) and relaxation rates (black diamonds) for 7 days after injection with a ACPPD-Gd similar to that in SI Scheme 1 except that (*i*) Suc-e_{10}-X replaced Suc-e_8-(PEG2); (*ii*) 10 copies of the ACPP instead of 6 were attached to each dendrimer; (*iii*) about 50 copies of DOTA-Gd rather than 15 were attached to each dendrimer; (*iv*) the final capping of the dendrimer attached about 68 rather than 104 copies of mPEG4. Intensities have been normalized to a water phantom. All data are normalized to the preinjection values at t = 0. Data are from four mice for the first three time points and three mice thereafter. (*B*) Similar relaxation rates and intensity data for liver. Again, intensities have been normalized to a water phantom and all data are normalized to the value at t = 0. T_1 values were obtained by varying T_r, taking five data points and fitting the resultant curve to Intensity = $A(1-\exp(1-T_r/T_1)$.

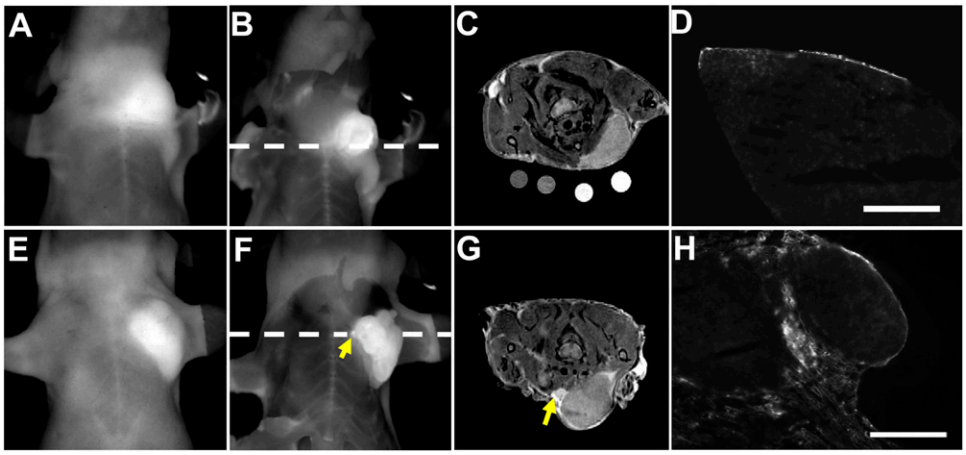

Fig. S7. Dual ACPPDs highlight borders of infiltrative HT-1080 xenografts. (*A–D*) Encapsulated HT-1080 xenograft resulting by s.c. implantation. (*E–H*) More infiltrative xenograft resulting from intramuscular implantation. (*A* and *E*) Fluorescence images through intact skin, 24 h after injection of cleavable dual ACPPD. (*B* and *F*) Corresponding images after removal of skin. (*C* and *G*) In vivo axial MRI slices at planes shown by dashed lines in *B* and *F*. Yellow arrows in *F* and *G* point to regions of infiltration. *C* also includes four phantoms containing 0, 10, 50, and 250 μM Gd-DTPA from left to right. (*D* and *H*) Higher magnification fluorescence images of frozen sections from encapsulated vs. infiltrative lesions, respectively. Intensity scaling is constant within each pairwise comparison (*A* vs. *D*, *B* vs. *E*, C vs. *F*, *D* vs. *G*). (*D* and *H* Scale bars, 1 mm.)

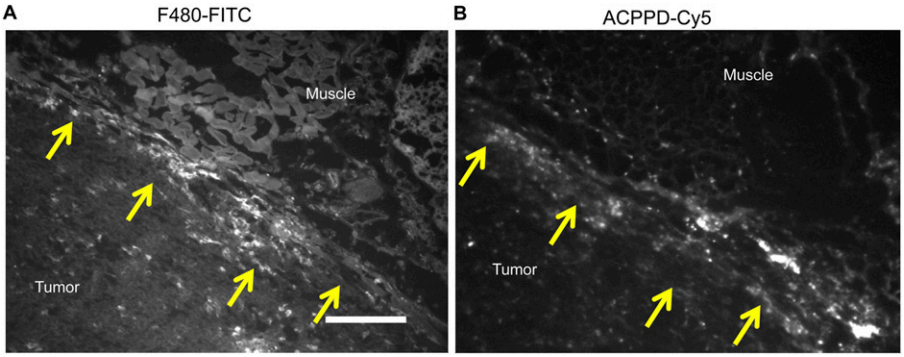

Fig. S8. F4/80 positive macrophages accumulate at infiltrative edges of tumors. (*A*) An F4/80 stained frozen section of a HT-1080 tumor in a mouse 48 h after injection with dual-ACPPD. (*B*) Dual-ACPPD accumulation at the edge of tumor in a similar section approximately 30–60 μm away. The interface between tumor and muscle is denotated by yellow arrows. Images have been scaled to max. (Scale bar, 200 μm.) (Magnification, 80×.)

Table S1. Standardized uptake and intensity values for various constructs in HT-1080 xenografts

	Payload	Tumor	Liver	Kidney	Muscle	Blood
SUV, Cleavable ACPPD (n = 8)	Cy5	1.8 (0.5)	2.9 (0.9)	0.8 (0.3)	0.2 (0.1)	nd
SUV, D-amino acid control ACPPD (n = 5)	Cy5	0.9 (0.2)	4.0 (0.5)	1.2 (0.4)	0.2 (0.1)	nd
SUV, Cleavable Free Peptide (n = 5)	Cy5	0.12 (0.07)	3.7 (1.2)	8.6 (1.4)	0.1 (0.03)	nd
SUV, Cleavable ACPPD (n = 5)	Gd	2.2 (0.4)	7.8 (1.0)	1.9 (0.7)	0.4 (0.2)	0.3 (0.1)* (n = 4)
SUV, D-amino acid control ACPPD (n = 4)	Gd	1.2 (0.2) (n = 3)†	4.2 (0.5)	1.4 (0.7)	0.2 (0.1)	0.5 (0.3)
Normalized Intensity, Cleavable ACPPD (n = 5)	Gd	1.21 (0.07)	1.06	nd	nd	nd
Normalized Intensity, D-amino acid control ACPPD (n = 3)	Gd	1.11 (0.01)	0.93 (n = 2)	nd	nd	nd

SDs are in parentheses. nd, not determined.
*Because of technical difficulties, blood was not collected from this animal.
†A single tumor was excluded because greater than 50% of the tumor volume was necrotic.